Journal of Magnetic Resonance 313 (2020) 106703

Contents lists available at ScienceDirect

Journal of Magnetic Resonance

journal homepage: www.elsevier.com/locate/jmr

Amplified detection of phosphocreatine and creatine after supplementation using CEST MRI at high and ultrahigh magnetic fields

KowsalyaDevi Pavuluri [a], Jens T. Rosenberg [b], Shannon Helsper [b,c], Shaowei Bo [a], Michael T. McMahon [a,d,*]

[a] The Russell H. Morgan Department of Radiology, The Johns Hopkins University School of Medicine, 991 N. Broadway Baltimore, MD 21205, USA
[b] The National High Magnetic Field Laboratory, CIMAR, Florida State University, Tallahassee, FL, USA
[c] Department of Chemical and Biomedical Engineering, FAMU-FSU College of Engineering, Tallahassee, FL, USA
[d] F.M. Kirby Research Center for Functional Brain Imaging, Kennedy Krieger Institute, 707 N. Broadway Ave., Baltimore, MD 21205, USA

ARTICLE INFO

Article history:
Received 9 November 2019
Revised 18 February 2020
Accepted 22 February 2020
Available online 27 February 2020

Keywords:
CEST imaging
Creatine
Magnetic resonance imaging
Molecular imaging

ABSTRACT

Creatine is an important metabolite involved in muscle contraction. Administration of exogenous creatine (Cr) or phosphocreatine (PCr) has been used for improving exercise performance and protecting the heart during surgery including during valve replacements, coronary artery bypass grafting and repair of congenital heart defects. In this work we investigate whether it is possible to use chemical exchange saturation transfer (CEST) MRI to monitor uptake and clearance of exogenous creatine and phosphocreatine following supplementation. We were furthermore interested in determining the limiting conditions for distinguishing between creatine (1.9 ppm) and phosphocreatine (2.6 ppm) signals at ultra-high fields (21 T) and determine their concentrations could be reliably obtained using Bloch equation fits of the experimental CEST spectra. We have tested these items by performing CEST MRI of hind limb muscle and kidneys at 11.7 T and 21.1 T both before and after intravenous administration of PCr. We observed up to 4% increase in contrast in the kidneys at 2.6 ppm which peaked ~30 min after administration and a relative ratio of 1.3 in PCr:Cr signal. Overall, these results demonstrate the feasibility of independent monitoring of PCr and Cr concentration changes using CEST MRI.

1. Introduction

Creatine (Cr) is an important metabolite found mostly in muscle and involved in muscle contraction. Since the discovery of phosphocreatine (PCr) and of the creatine kinase (CK) reaction in 1927 and 1934 respectively, research efforts have focused on its involvement in energy metabolism [1]. In fast twitch skeletal muscles, PCr stores phosphate for regeneration of adenosine triphosphate (ATP) from adenosine diphosphate (ADP) during high intensity, short duration activity and is converted to creatine (Cr) during this reaction. Because of this, Cr is regularly taken by athletes around the country as a nutritional supplement for performance enhancement, indeed it has been reported that all the National Football League teams have between 33 and 90% of their players using Cr supplementation [2–4]. Besides this, some researchers have observed that PCr supplementation can be protective following heart surgery including for surgical valve replacements, coronary artery bypass grafting and repair of congenital heart defects [5,6]. One of the challenges of supplementation is that there are large differences in dosage and duration between supplementation protocols, while methods which can assess Cr and PCr content in various organs of interest which would be helpful to evaluate the benefits are lacking.

Molecular imaging enables a detailed understanding of biological function through detection of the distribution of important compounds in biological pathways [7], and can be accomplished using strategies which detect unaltered, natural compounds and their metabolites. MRI and MRSI are uniquely valuable tools within the field of molecular imaging for visualizing the spatial distribution of metabolites in soft tissue. Cr, PCr and creatinine (Crn) are the three compounds found in creatine metabolism, and possess several nuclei detectable via NMR (Fig. 1). While ^{1}H, ^{31}P and ^{13}C based MRSI have all been used for monitoring their presence in tissue [8–14], unfortunately MRSI presents disadvantages for widespread application. In the case of ^{31}P MRSI the image resolution has limitations based on sensitivity, only PCr can be measured and ^{31}P MRSI requires specialized hardware and software. For ^{1}H MRSI, only total creatine is quantified instead of the three individual compounds due to limited spectral resolution. Based on this

* Corresponding author at: F.M. Kirby Research Center for Functional Brain Imaging, Kennedy Krieger Institute, 707 N. Broadway Ave., Baltimore, MD 21287, USA.
E-mail address: mcmahon@kennedykrieger.org (M.T. McMahon).

https://doi.org/10.1016/j.jmr.2020.106703
1090-7807/

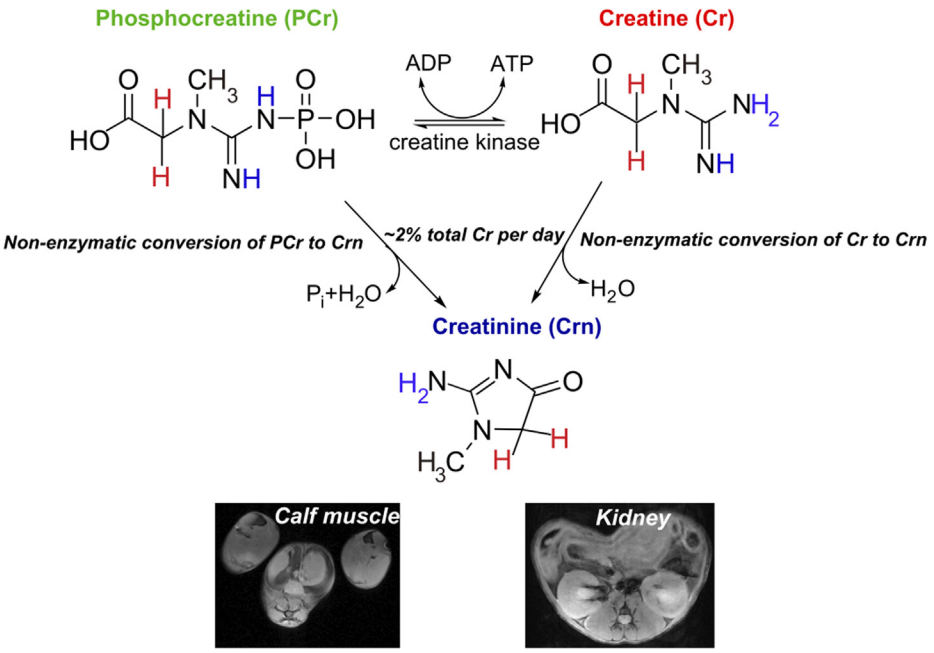

Fig. 1. Important molecules involved in creatine metabolism including CEST detectable protons (blue) and MRS detectable protons (red). Creatine has 3 equivalent labile protons, phosphocreatine has 1 equivalent labile proton (1 nonequivalent) and creatinine has 2 equivalent labile protons. (Lower panel) representative axial MRI of calf muscle and kidneys, two locations for detecting these metabolites. (For interpretation of the references to colour in this figure legend, the reader is referred to the web version of this article.)

there is a need for new noninvasive methods to quantify creatine metabolism in tissue.

Chemical exchange saturation transfer (CEST) contrast represents an attractive method for amplified detection of important compounds in biological pathways using the MRI saturation signatures of exchangeable protons [15–22]. Indeed, a number of molecules have been reported as elegant examples of diamagnetic CEST (diaCEST) agents including urea [23,24], glucose [25,26], glutamate [27,28], Cr [29–31], glycosaminoglycans [32,33], barbituric acid [34,35], triiodobenzenes [36–39], thymidine analogues [40] salicylates [41], anthranillates [42], imidazoles [43] and free base porphyrins [44]. In addition, several peptides and proteins have been optimized as CEST reporter genes including lysine rich protein and protamine [45–48]. Herein, we show that it is possible to specifically follow the uptake and clearance of Cr and PCr separately via CEST MRI and demonstrate these concentrations can be modeled using multiple pool Bloch equations.

2. Methods

Phantom Preparation and CEST Experiments: All samples were dissolved in 0.01 M phosphate-buffered saline (PBS) at 25 mM concentrations and titrated to the pH values 6.2, 6.5, 6.8 and 7.1 using high concentration HCl/NaOH. The solutions were placed into 5 mm NMR tubes and assembled in a holder for CEST MR imaging. The samples were kept at 37 °C during imaging. 11.7 T phantom data were acquired on a Bruker vertical MR scanner (Bruker Avance, Ettlingen, Germany) using a 25 mm transmit/receive coil and the RARE sequence (RARE Factor = 32). CW saturation pulse length = 3 sec, saturation field strength (B_1) = 1.0 μT to 6 μT. The CEST Z-spectra were acquired by incrementing the saturation frequency every 0.12 ppm from −5.5 to 5.5 ppm. WASSR images were also acquired using a 3 sec CW saturation pulse with B_1 = 0.5 μT, saturation frequency incremented from −1.5 ppm to 1.5 ppm. 21.1 T phantom CEST experiments were performed on 25 mM solutions in 0.01 M PBS as well. These CEST images were recorded on a 21.1 T vertical MR scanner [49] equipped with a Bruker Avance III console (Bruker Corp. Ettlingen, Germany). A home-built 35 mm transmit/receive coil was used for all experiments. CEST images were acquired using a RARE (RARE Factor = 12; effective TE = 3.58 ms) sequence with CW saturation pulse length of 3 s and B_1 from 1.0 μT to 6 μT. The CEST Z-spectra were acquired for 85 offsets between −5 and +5 ppm and one M_0 offset. Other parameters were kept same between 11.7 T and 21.1 T and were: TR = 6 s, effective TE = 4.5 ms, matrix size = 64 × 64 and slice thickness of 1.5 mm.

Animal Imaging: All animal experiments were performed under protocols approved by the Johns Hopkins University Animal Care and Use Committee and the Florida State University Animal Care and Use Committee. C57Bl/6 mice weighing 30–35 gr were used for all experiments. The 11.7 T Bruker Biospec at John Hopkins and the 21.1 T scanner at the National High Magnetic Field laboratory (NHMFL) were used to collect the images in this study through Paravision 6.0.1. On the 11.7 T scanner, a 70 mm transmit coil and an 8 channel mouse body phase array coil were used for collecting MRI data. On the 21.1 T scanner, the 35 mm transmit/receive volume coil was used for collecting MRI data. After confirming accurate placement of the mice in the coil, shimming was performed using a localized voxel placed over the left and right kidneys. The RARE sequence was used for all images. *In vivo* B_0 inhomogeneity maps were generated from the WASSR experiment performed before the injection for each mouse. WASSR Z-spectra for ROI's drawn over both the kidneys were extracted and interpolated in Matlab using cubic spline interpolation. The water shift was measured pixel by pixel as described previously [50,51] to obtain the ΔB_0 maps over the kidney. For muscle and kidney CEST images collected without administering PCr, a 3 sec CW saturation pulse was used and CEST images were acquired with saturation B_1 = 1, 1.5, 2, and 2.5 μT. Z-spectra were collected at 81 saturation frequencies between −5 and +5 ppm and one additional at +40 ppm for determining M_0. Other experimental parameters include: TR = 10 sec, effective TE = 27.9 ms, matrix = 48 × 32, slice thickness = 1.5 m m. For the PCr administered experiments at 21.1 T, a micro cannula was inserted in the lateral tail vein of the mouse and secured for

insertion into the magnet in order to inject 150 μl of 325 mM PCr at neutral pH during the MRI experiments. Prior to start of the CEST experiment, shimming was performed and a 1-mm thick axial slice was placed to bisect the center of the major calyces on both kidneys. CEST images were collected at 9 frequencies in this study (1.6, 1.8, 1.9, 2.1, 2.2, 2.4, 2.6, 2.7, 2.9 ppm) repetitively (each frequency was collected 85 times for a total of 9*85 = 765 images). Each offset was acquired in one-shot using repetition time (TR) = 8 s. The saturation preparation consisted of 15 pulses with block shape (bp) that were 200 ms long resulting in a 3 s saturation pulse train at B_1 = 2.5 μT. CEST images acquired using this oversampling approach allows for correction of motion artifacts during the 1 h 40 min scan through data temporal averaging (smoothing) as described previously [52]. The injection of PCr occurred at 8 min following start of the acquisition to allow robust acquisition of pre-injection images.

Data Processing: In vitro and *in vivo* CEST MRI data were processed using custom written Matlab code. *In vitro* mean Z-spectra and MTR_{asym} were calculated by drawing an ROI over each phantom tube. QUESP and Bloch simulations were used to fit the data and extracting the exchange rates at each pH value as described previously [53]. *In vivo* muscle mean Z-spectra were produced and the baseline Z-spectrum without the PCr and Cr CEST peaks was calculated using spline interpolation and subtracted from the mean Z-spectra to calculate the difference (contrast) spectra for n = 3 mice on the 11.7 T scanner and n = 3 mice on the 21.1 T scanner. For calculating this difference spectra, one additional half width of the CEST peak from the lowest point on either side of these peaks was used to define the range of the peak. The mean Z-spectrum over an ROI covering the muscle was fit using 4 pool Bloch simulations (PCr, Cr, MT, water pools) to simulate the MT effect for calculating the water T_1 and T_2 values with parameters listed in Table 2, with errors estimated through Monte Carlo error estimation using 1000 iterations. Using these values, the muscle contrast spectra were fit to determine the *in vivo* PCr and Cr concentrations without administration of PCr. The *in vivo* kidney data for ROIs which exclude the collecting system were processed in a similar manner. For analyzing the 21.1 T Z-spectra without administering PCr, the mean Z-spectra were extracted and difference spectra calculated. The difference spectra were calculated in a similar manner as muscle, by allowing a half width space on each side of the CEST peaks and fitting these difference spectra using 4 pool Bloch simulations to calculate the Cr and PCr concentrations in kidney (Table 2). For the 21.1 T dynamic CEST contrast results, the mean Z-spectra of both pre and post contrast were extracted. The mean pre-injection z-spectra were subtracted from all post-injection images. For this dynamic data set, the 'smooth' function in Matlab was used to apply a moving time average to remove the motion induced fluctuations in the dynamic CEST contrast data as described previously [52]. The smoothening factor used in the averaging process was ~10 neighboring images, with this choice based on the size of the data and the range of fluctuations. After smoothening ~2–3 images were averaged to generate the CEST contrast maps. Maximum contrast maps were generated by calculating the pixel-by-pixel ST ($1-M_z/M_0$) on two ROIs, one over each kidney, overlaid on the corresponding T2W image. CEST dynamic contrast build up curve at two offsets correspond to Cr and PCr was obtained on the 21.1 T scanner by taking the average of the CEST build up curves for n = 6 mice.

3. Results

We were interested first in comparing how ^{1}H NMR and ^{1}H CEST would perform for detecting these metabolites. As is seen in Fig. 2, Table 1, there are some difficulties discriminating the

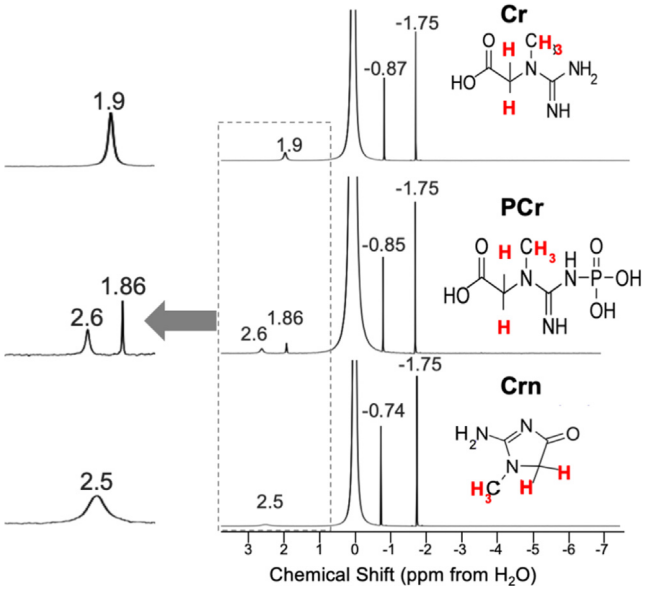

Fig. 2. ^{1}H NMR spectra for Cr, PCr, Crn. Conditions: pH ~ 6.5, 10%/90% D_2O/H_2O at T = 20 °C.

Table 1
Chemical shifts of labile protons for the compounds in this study.

Compound	Chemical shift (ppm)	Chemical shift (ppm)
Creatine	NH_2: 1.9 ppm	NH: 1.9 ppm
Phosphocreatine	NH: 1.86 ppm	NH: 2.6 pm
Creatinine	NH_2: 2.5 ppm	

three metabolites, as the ^{1}H NMR spectra for all three consists of two peaks with the CH_3 resonating at −1.75 ppm from H_2O for all three. As is shown, there are small differences for the CH_2 which for Cr is −0.87 ppm while PCr resonates at −0.85 ppm and Crn a little removed at −0.74 ppm. Because of this, for MRS studies total creatine is quantified instead [13]. This contrasts with the CEST Z-spectra of Cr, PCr and Crn (Fig. 3A and B) which displays peaks at 1.9 ppm, 2.6 ppm and 2.5 ppm respectively. Although Crn is not so well separated, this is a very low concentration species, as ~2% of total Cr in muscle is converted to Crn per day [1] and as a result Crn is not expected to contribute to signal in tissue. There are also peak intensity differences observed. Cr possesses 3 labile protons per molecule, PCr possesses 2 NH and CrN possesses 2 NH and there are also exchange rate (k_{ex}) differences for these labile protons which impact this sensitvity. As is shown in Fig. 3A and B, at 11.7 T the most sensitive compound is Cr using moderate saturation pulses (B_1 = 1.5 μT) as is expected based on the factor of 1.5 larger labile proton content. We performed QUESP experiments to measure these rates (Fig. 3C and D) which revealed the fastest exchanging protons were found on Crn, followed by Cr and PCr with the k_{ex}'s being pH dependent. Also as is shown in PBS in Fig. 3C, increasing the B_1 from 1 to 4 μT results in larger signal enhancements for PCr and Cr. Unfortunately, use of stronger saturation pulses results in overlap of the 1.9 ppm and 2.6 ppm peaks for these two metabolites. We performed a second round of phantom experiments with the phantom consisting of tubes with 5 different concentrations, 50, 25, 20, 10, 5 mM of Cr and PCr. The resulting difference spectra were fit to determine the concentrations as described in the methods section with the results shown in Fig. 3E and F. We observed a linear correlation between the spectral fit determined concentration and measured concentrations with rmsd < 1 mM for both Cr and PCr indicating the suitability

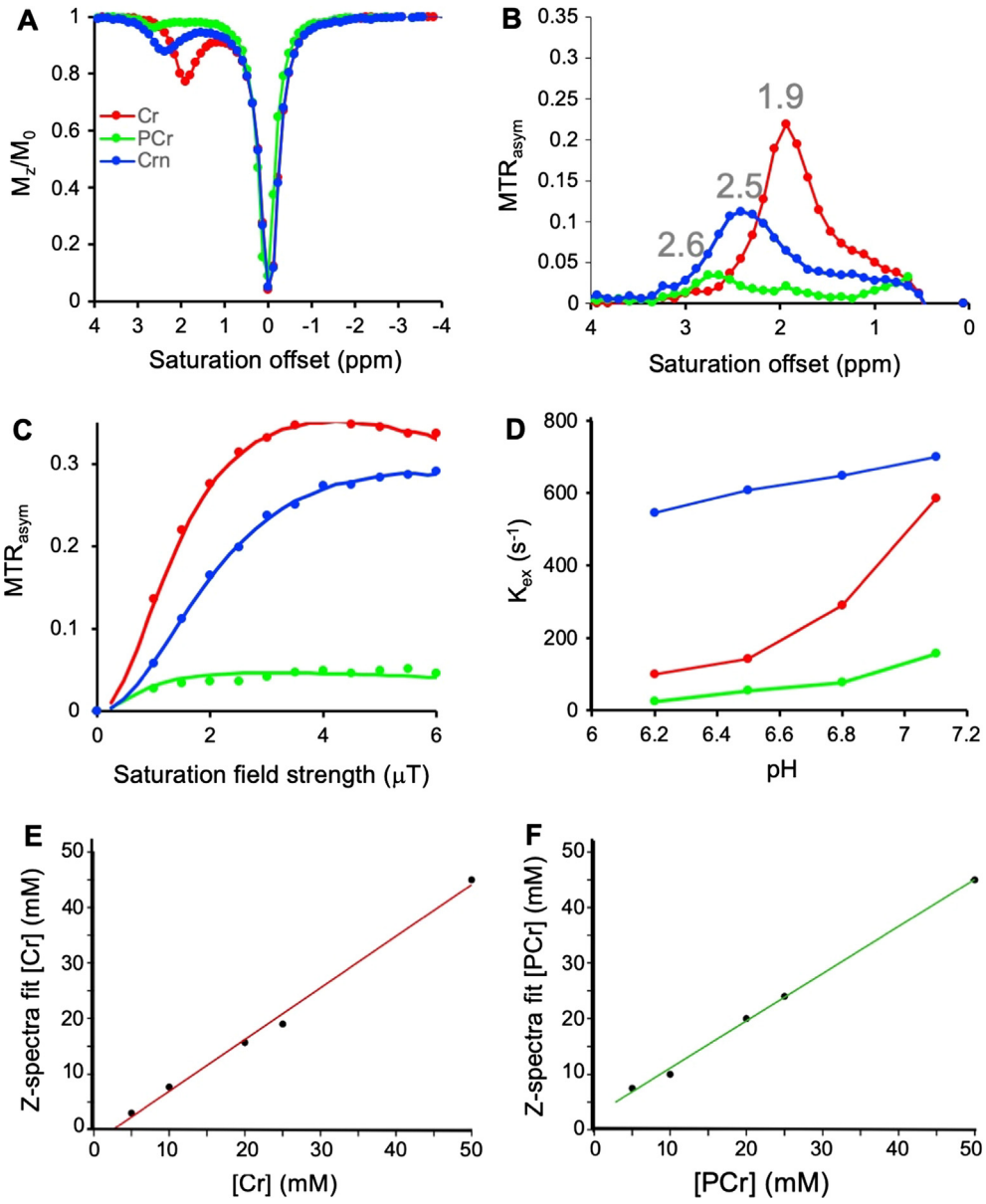

Fig. 3. *In vitro* phantom results. (A) CEST Z-spectra and (B) MTR_{asym} of Cr, PCr and Crn using B_1 = 1.5 μT; (C) QUESP plots of Cr, PCr and Crn at pH 7.1 obtained with B_1 = 1, 1.5, 2, 2.5, 3, 3.5, 4, 4.5, 5, 5.5 and 6 μT respectively; (D) Exchange rate vs pH of Cr, PCr and Crn measured using Bloch simulation fitting the QUESP dataset; (E) Correlation between spectral fit concentration and measured concentrations for [Cr] = 50, 25, 20, 10, 5 mM; (F) Correlation between spectral fit concentration and measured concentrations for [PCr] = 50, 25, 20, 10, 5 mM; Conditions: 20 mM Cr, PCr, and Crn phantoms, T = 37 °C and pH values 6.2, 6.5, 6.8 and 7.1 were used for CEST experiments.

of our fitting methods over this range in concentrations. In order to determine what saturation conditions are ideal for sensitively detecting Cr and PCr and minimizing overlap, we performed a series of Bloch simulations (Fig. 4A). As is shown, minimal overlap can be achieved at 11.7 T using 1.5 μT saturation pulse trains, representing a good balance of sensitivity and resolution. This results in an enhancement in detection of ~200 for Cr and ~165 for PCr at neutral pH as calculated previously [54]. Based on the same simulations, at 21.1 T we can achieve larger enhancements of ~350 and 200 for Cr, PCr while retaining good spectral resolution by using 2.5 μT saturation pulse trains as can be observed from the Z-spectra and asymmetry spectra at 21.1 T shown in Fig. 4B,C and as quantified in Fig. 4A which indicates a 0.5% increase in PCr contrast due to the 1.9 ppm Cr peak. Based on our results which show that CEST detection of Cr and PCr results in enhanced resolution over ^{1}H NMR and also enhanced detection, we moved to *in vivo* studies.

Next, we moved to determining whether we could quantify the amount of these compounds in tissue using CEST imaging in healthy C57Bl/6 mice. Based on *in vivo* monitoring of [4-^{13}C] creatine injected mice, muscle possesses ~22.5 mM PCr and ~7.5 mM Cr, fairly large concentrations of these metabolites which should render these detectable by CEST imaging [12]. Fig. 5 shows CEST MRI Z-spectra acquired on calf muscle at both 11.7 T (Fig. 5A) and 21.1 T (Fig. 5C), revealing two separate peaks for Cr and PCr at both field strengths. In order to quantify the concentrations, we fit the baseline around these two peaks to a 3rd order polynomial and subtracted this from the Z-spectra similar to the three point analysis performed by Tao and colleagues [55]. Fig. 5(B and D) displays the resulting processed experimental data with Cr displaying a stronger signal than PCr at both 11.7 and 21.1 T despite the 3 fold lower concentration in tissue from previous studies[12]. As is also seen, at 21.1 T there was enhanced resolution of the two peaks as expected. Based on fitting this data to numerical solutions to four

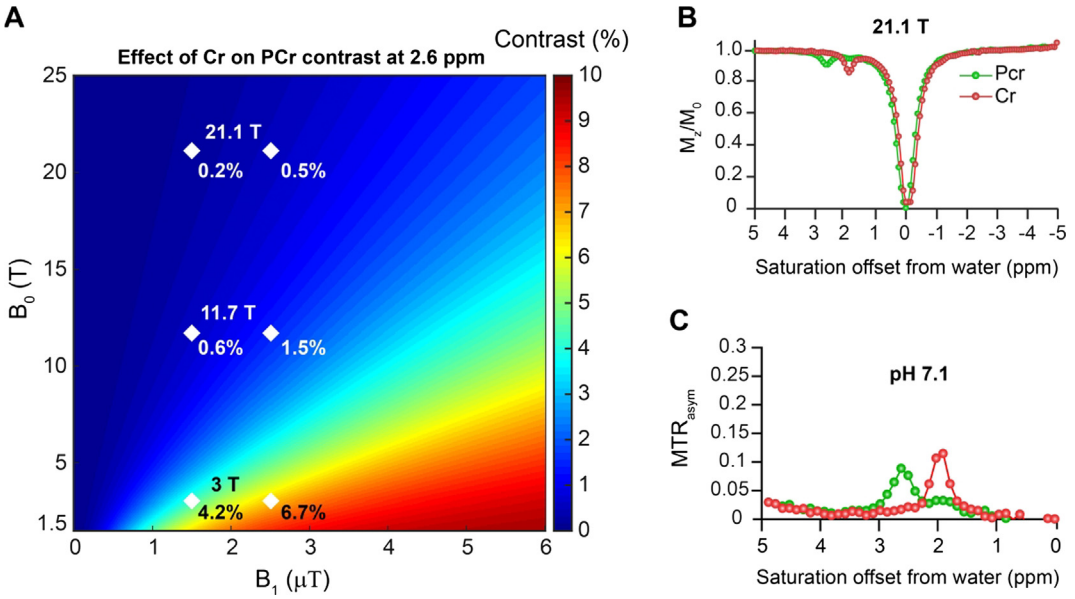

Fig. 4. Bloch simulations of Cr, PCr contrast and *in vitro* CEST experiments on phantoms at 21.1 T. (A) Bloch simulations of increase in PCr contrast due to presence of the 1.9 ppm Cr peak at different B_0 and B_1 fields. Diamonds are shown at the critical values of B_1 = 1.5 μT and 2.5 μT to indicate that the PCr CEST contrast at 2.6 ppm is increased by 4.2%, 0.6% and 0.2% by overlap with 1.9 ppm Cr peak for B_1 = 1.5 μT and to 6.7%, 1.5% and 0.5% for B_1 = 2.5 μT on 3, 11.7 and 21 T MRI scanners respectively. T_1 and T_2 relaxations were kept constant for simulations as mentioned in Table 2; (B) 21.1 T CEST Z-spectra and (C) 21.1 T MTR_{asym} spectra of Cr, PCr samples at pH 7.1, T = 37 °C using 2.5 μT RF saturation.

pool Bloch equations using the k_{ex} determined in Fig. 3, we estimated the concentrations of Cr and PCr to be 10.8 mM, 19.5 mM (11.7 T) and 10.7 mM, 15.8 mM (21.1 T) with all parameters listed in Table 2 which is in excellent accord with the literature [12]. As is also seen in Fig. 5, we were able to achieve a good fit (rmsd < 0.002) of the experimental muscle data at both 11.7 T and 21.1 T. Finally, we can also produce pixelwise contrast/difference maps at both PCr and Cr (Fig. 5E and F) frequencies revealing relatively homogeneous distribution of both through muscle tissue. If the muscle pH were to drop from 7.1 to 6.5, an error in concentration would be observed (Table 2) with measurements ranging from 9.6 to 17 mM for Cr and from 16 to 40 mM for PCr, however based on the literature we don't expect muscle pH to go below 7.0 during exercise [56]. These results show excellent agreement between prior [4-^{13}C] creatine measurements [12] and CEST MRI, and excellent detection of Cr and PCr prior to supplementation.

Finally, we tested how well we could detect creatine signal in the kidney and changes in these signals after PCr supplementation (Fig. 6). As is shown, the kidney also displays pronounced signals at PCr and Cr resonances, although these are broader than found in calf muscle (Fig. 6A and B) which may be due to different metabolites such as glutamine, alanine and ammonia contributing to these resonances [23,57]. Again the fits of these two peaks using the parameters in Table 2 displayed excellent agreement with the experiments. We injected 325 mM PCr in saline into the tail vein of mice and monitored the PCr and Cr signals with time (Fig. 6C and D) by subtracting the pre-injection images at these offsets to remove the potential impact of additional metabolites. Peak contrast of ~4.6% was achieved earlier for PCr (~30 min) than for Cr (~3.8% at 40 min) in the medulla as is shown. Based on comparing with pre-injection and using the parameters in Table 3, this represents an increase in PCr of ~187 mM and increase of in Cr of ~23 mM.

4. Discussion

In this study, we have tested the field dependence of CEST MRI detection of PCr and Cr both from Bloch simulations and experiments up to 21.1 T. We have shown that it is possible to obtain the Cr and PCr concentrations directly from fitting the CEST Z-spectra using numerical solutions to the Bloch equations at multiple magnetic field strengths. This approach is different from that of previous studies by Balaban, Reddy, Vandsburger, Xu, Sun, Jin and colleagues who have been interested in detecting endogenous Cr and PCr concentrations at lower magnetic field strengths [23,29–31,58–61]. While monitoring signal intensity or performing lorentzian line-shape fitting could also be used to quantify concentration, as we show use of Bloch simulation fits results in numbers which are in good accord with literature values in muscle tissue and furthermore has the advantage that these allow testing how the concentration measurements are impacted by changes in tissue pH. Our approach for isolating these peaks is similar to the three point analysis method used by Jin and colleagues [55], however it diverges in that we use more frequency points. Muscle pH has been measured to drop from pH 7.3 to 6.9 in the cases of hemorrhage, hypoxia, hypothermia and exercise and in the extreme case of limb ischemia when blood flow was clamped for 2 hrs the muscle pH dropped to pH 6.55 [56,62]. Indeed, using 4 pool Bloch equation fits we found that if there was a significant hemorrhage or ischemia in the imaged region, the PCr concentration measurements would be substantially altered but Cr measurements would be not so impacted. Cr concentration measurements are less effected by pH compared to that of PCr because of the impact changes in k_{ex} have on contrast for $k_{ex} \sim 500\ s^{-1}$ compared to when $k_{ex} \sim 100\ s^{-1}$ which also results in larger errors for the fast k_{ex} measurements similar to what we have found previously [53] and is seen in Table 2. Based on this, our approach should result in a reasonable range of concentration errors of < 10% for Cr and < 20% for PCr as long as there is not prolonged limb ischemia.

We have also investigated use of natural PCr, a nutritional supplement, as a CEST agent and that there is specific enhancement at both Cr and PCr frequencies after intravenous administration. We compared post-injection images to those acquired over 8 min pre-injection to deconvolute the influence of PCr supplementation from other factors, although it is possible that hydration status due to injection of fluid may have some impact. The impact of hydra-

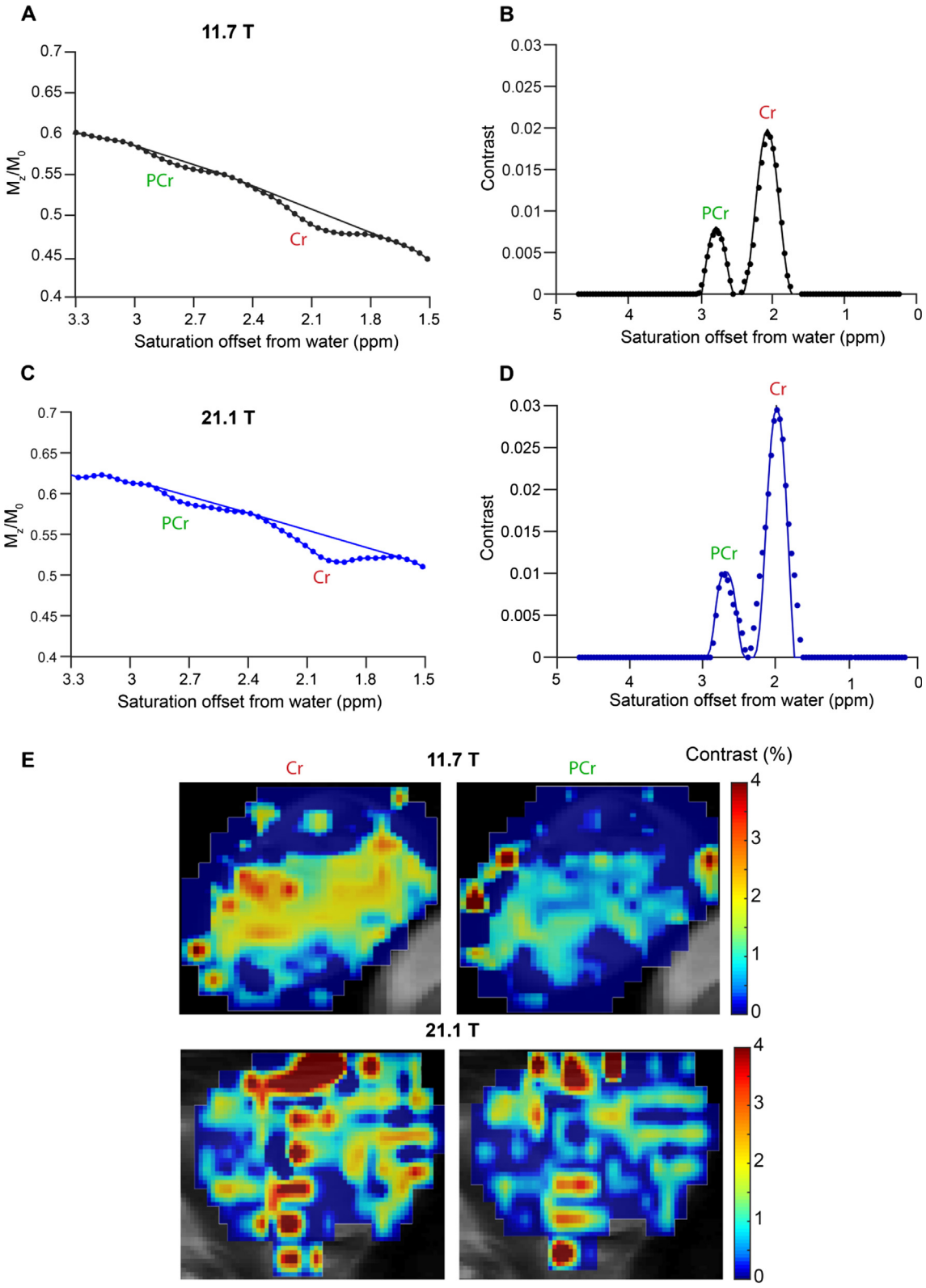

Fig. 5. Comparison between 11.7 T and 21.1 T muscle CEST contrast of Cr and PCr. (A) Z-spectrum from an ROI drawn over the muscle of a mouse, CEST data was acquired at B_1 = 1.5 μT on 11.7 T scanner. A polynomial data generated by removing the CEST contrast was fit to separate the CEST contrast of Cr and PCr; (B) The difference spectrum displayed between 0 and 5 ppm of saturation offsets. This difference spectrum was obtained by subtracting from the experimental Z-spectrum a 3rd order polynomial fit to the experimental spectrum minus the PCr and Cr peaks to determine the Cr and PCr concentrations in mouse muscle which were 10.8 mM and 19.5 mM respectively; (C) Z-spectrum from an ROI drawn over the muscle of a mouse with CEST data acquired at B_1 = 1.5 μT on 21.1 T scanner; (D) Difference spectrum obtained by subtracting from the experimental Z-spectrum a 3rd order polynomial fit to the experimental spectrum minus the PCr and Cr peaks. The concentrations of Cr and PCr in muscle were found to be 10.7 and 15.8 mM respectively based on Bloch simulation fittings of the 21.1 T data; (E) 11.7 and 21.1 T CEST contrast maps at Cr and PCr frequencies for a single calf muscle.

Table 2
Bloch simulation parameters for muscle Cr and PCr concentration calculations on 11.7 and 21.1 T scanners.

	Muscle	11.7 T scanner		
Parameter	Water	MT pool (A)	Cr pool (B)	PCr pool (C)
Δω (ppm)	0	0	1.9	2.6
R_1 (s^{-1})	1/(2 ± 0.7)	1	1	1
R_2 (s^{-1})	1/(0.033 ± 0.001)	$1/15 \times 10^{-6}$	1/(0.5 ± 0.1)	1/(0.5 ± 0.1)
Mol (mM)	110,000	11.7		
pH 6.5			14.2	41.5
pH 6.8			9.6	30.7
pH 7.1			10.8	19.5
k_{ex} (/sec)	–	21		
pH 6.5			143 ± 15	55 ± 3
pH 6.8			292 ± 50	78 ± 6
pH 7.1			585 ± 150	158 ± 15
	Muscle	21. 1 T scanner		
Parameter	Water	MT pool (A)	Cr pool (B)	PCr pool (C)
Δω (ppm)	0	0	1.9	2.6
R_1 (s^{-1})	1/(2.33 ± 0.06)	1	1	1
R_2 (s^{-1})	1/(0.015 ± 0.0004)	$1/15 \times 10^{-61}$	1/(0.3 ± 0.1)	1/(0.3 ± 0.1)
Mol (mM)	110,000	11.7		
pH 6.5			17.5	37.7
pH 6.8			11	28
pH 7.1			10.7	15.8
k_{ex} (/sec)	–	21		
pH 6.5			143 ± 15	55 ± 3
pH 6.8			292 ± 50	78 ± 6
pH 7.1			585 ± 150	158 ± 15

[1] R_1, R_2 values of MT, Cr, PCr without error estimates are similar to those found in Ref. [15].

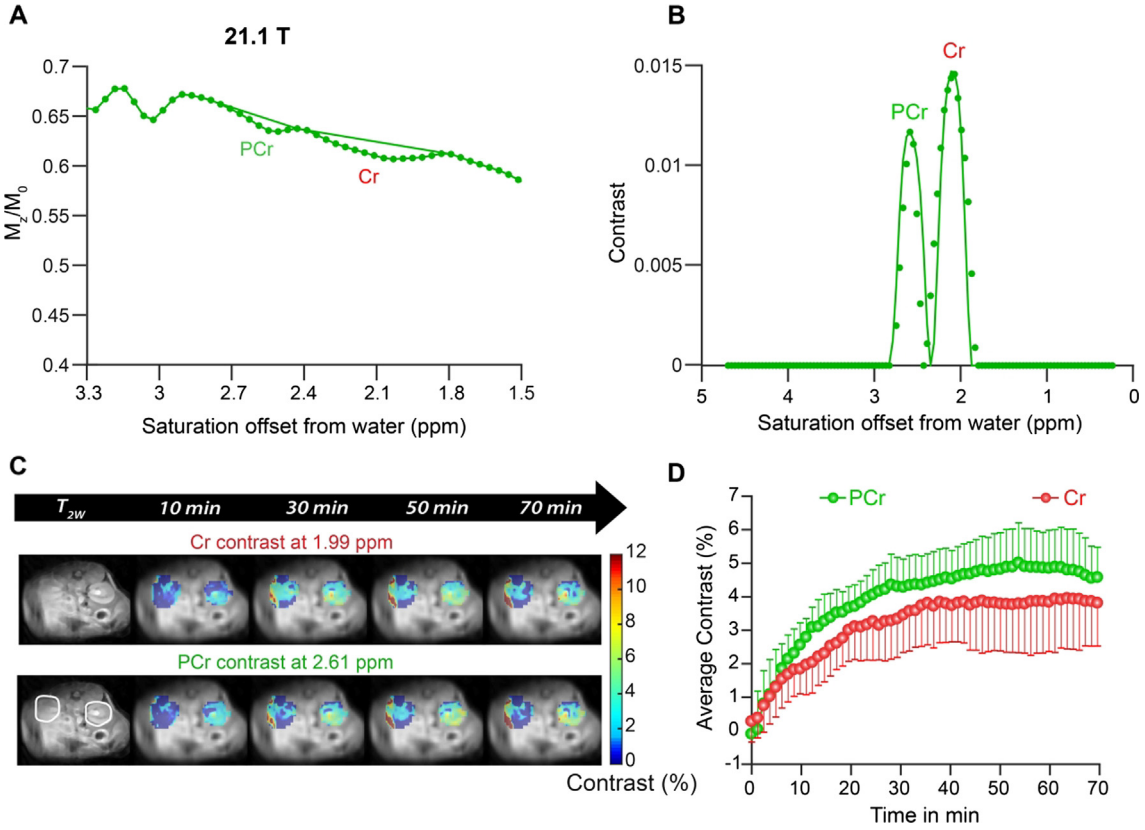

Fig. 6. *In vivo* kidney CEST experiments on 21.1 T scanner on mice. (A) Z-spectrum and 3rd order polynomial prior to PCr injection for an ROI drawn over the cortex of the kidney which avoided the collecting system. Cr and PCr contrast can be seen clearly at 1.99 and 2.61 ppm respectively; (B) The difference spectrum calculated by subtracting the experimental Z-spectrum and the polynomial with experimental data (symbols) and fit (solid lines) to obtain the *in vivo* Cr and PCr concentrations = 6 mM and 22.5 mM respectively; (C) *In vivo* kidney dynamic CEST contrast images overlaid on high resolution T_{2W} images at 21.1 T after administering 325 mM PCr. ST = 1-M_z/M_0 at 1.9 and 2.6 ppm corresponds to Cr and PCr frequencies; (D) Average CEST contrast of Cr and PCr after administering PCr to healthy mice [n = 6] and acquiring *in vivo* CEST kidney data at 21.1 T. Both Cr and PCr uptake peaked between 20 and 40 min.

Table 3
Bloch simulation parameters for kidney Cr and PCr concentration calculations on 21.T scanner.

Kidney cortex		21.1 T scanner		
Parameter	Water	MT pool (A)	Cr pool (B)	PCr pool (C)
$\Delta\omega$ (ppm)	0	0	1.9	2.6
R_1 (s^{-1})	1/3.1	1	1	1
R_2 (s^{-1})	1/0.028	$1/15 \times 10^{-6}$	1/0.5	1/0.5
Mol (mM)	–	11.7	8.9	47.9
k_{ex} (/sec)	–	21	143	55

tion between post-injection and pre-injection is expected to be minimal based on the volume injected although this wasn't explicitly evaluated. Our methodology of collecting CEST spectra of the regions of interest and determining concentrations using Bloch equation fits is applicable to monitor a wide variety of creatine or phosphocreatine supplementation protocols in use. Based on our experiments, this CEST imaging based approach presents two main advantages over MRS: (1) CEST doesn't require isotopic enrichment of the supplement for discriminating between Cr and PCr in the spectra; (2) saturation transfer results in significant amplification factors (160 and higher) as shown experimentally at 11.7 T and 21.1 T to improve detection. Other investigators have reported ~5–500% changes in total creatine tissue concentrations through supplementation with the amount varying depending on dosage, frequency and tissue type [63] and we expect that changes in tissue Cr and PCr concentrations on that order could be spatially visualized and accurately quantified using our methods without need for invasive biopsy. As we show, the amplification of the signal is dependent on the magnetic field used for imaging, with higher fields allowing larger amplification factors while maintaining Cr and PCr peak resolution. We believe this approach should allow improvements in creatine supplementation protocols through direct monitoring of metabolite concentrations and quantification of creatine metabolism in response to muscle usage.

5. Conclusion

In conclusion, we have demonstrated that CEST detection of Cr and PCr is fairly robust over a wide range of experimental conditions and magnetic field strengths and that Bloch simulations allow robust quantification of these important compounds in phosphate storage. Improvements were seen using ultra high field magnets in terms of contrast (~33%, 20% increase in Cr, PCr contrast respectively) and in spectral resolution.

Declaration of Competing Interest

The authors declare that they have no known competing financial interests or personal relationships that could have appeared to influence the work reported in this paper.

Acknowledgements

This work was supported in part by P41EB024495. The National High Magnetic Field Laboratory is supported by the National Science Foundation through NSF/DMR-1644779 and the State of Florida, USA.

References

[1] M. Wyss, R. Kaddurah-Daouk, Creatine and Creatinine Metabolism, Physiol. Rev. 80 (3) (2000) 1107–1213.
[2] R.B. Kreider, D.S. Kalman, J. Antonio, T.N. Ziegenfuss, R. Wildman, R. Collins, D. G. Candow, S.M. Kleiner, A.L. Almada, H.L. Lopez, International Society of Sports Nutrition position stand: safety and efficacy of creatine supplementation in exercise, sport, and medicine, J. Int. Soc. Sports Nutr. 14 (1) (2017) 18.
[3] J.M. Tokish, M.S. Kocher, R.J. Hawkins, Ergogenic aids: A review of basic science, performance, side effects, and status in sports, Am. J. Sports Med. 32 (6) (2004) 1543–1553.
[4] D. Olson, R.S. Sikka, A. Labounty, T. Christensen, Injuries in Professional Football: Current Concepts, Curr Sport Med Rep 12 (6) (2013) 381–390.
[5] M. Cisowski, A. Bochenek, E. Kucewicz, A.M. Wnuk-Wojnar, W. Morawski, J. Skalski, H. Grzybek, The use of exogenous creatine phosphate for myocardial protection in patients undergoing coronary artery bypass surgery, The Journal of cardiovascular surgery 37 (6 Suppl 1) (1996) 75–80.
[6] C. Guo-han, G. Jian-hua, H. Xuan, W. Jinyi, L. Rong, L. Zhong-min, Role of creatine phosphate as a myoprotective agent during coronary artery bypass graft in elderly patients, Coron. Artery Dis. 24 (1) (2013) 48–53.
[7] T.F. Massoud, S.S. Gambhir, Molecular imaging in living subjects: seeing fundamental biological processes in a new light, Genes Dev. 17 (5) (2003) 545–580.
[8] P.A. Bottomley, R.G. Weiss, Non-invasive magnetic-resonance detection of creatine depletion in non-viable infarcted myocardium, Lancet (London, England) 351 (9104) (1998) 714–718.
[9] M. Beer, T. Seyfarth, J. Sandstede, W. Landschutz, C. Lipke, H. Kostler, M. von Kienlin, K. Harre, D. Hahn, S. Neubauer, Absolute concentrations of high-energy phosphate metabolites in normal, hypertrophied, and failing human myocardium measured noninvasively with (31)P-SLOOP magnetic resonance spectroscopy, J. Am. Coll. Cardiol. 40 (7) (2002) 1267–1274.
[10] S. Neubauer, M. Beer, W. Landschutz, J. Sandstede, T. Seyfarth, C. Lipke, H. Kostler, T.W. Pabst, M. Meininger, M. von Kienlin, M. Horn, K. Harre, D. Hahn, Absolute quantification of high energy phosphate metabolites in normal, hypertrophied and failing human myocardium, Magma (New York, NY) 11 (1–2) (2000) 73–74.
[11] I. Nakae, K. Mitsunami, T. Omura, T. Yabe, T. Tsutamoto, S. Matsuo, M. Takahashi, S. Morikawa, T. Inubushi, Y. Nakamura, M. Kinoshita, M. Horie, Proton magnetic resonance spectroscopy can detect creatine depletion associated with the progression of heart failure in cardiomyopathy, J. Am. Coll. Cardiol. 42 (9) (2003) 1587–1593.
[12] H.J. 't Zandt, A.J. de Groof, W.K. Renema, F.T. Oerlemans, D.W. Klomp, B. Wieringa, A. Heerschap, Presence of (phospho)creatine in developing and adult skeletal muscle of mice without mitochondrial and cytosolic muscle creatine kinase isoforms, J. Physiol. 548 (Pt 3) (2003) 847–858.
[13] G. Öz, J.R. Alger, P.B. Barker, R. Bartha, A. Bizzi, C. Boesch, P.J. Bolan, K.M. Brindle, C. Cudalbu, A. Dinçer, U. Dydak, U.E. Emir, J. Frahm, R.G. González, S. Gruber, R. Gruetter, R.K. Gupta, A. Heerschap, A. Henning, H.P. Hetherington, F. A. Howe, P.S. Hüppi, R.E. Hurd, K. Kantarci, D.W.J. Klomp, R. Kreis, M.J. Kruiskamp, M.O. Leach, A.P. Lin, P.R. Luijten, M. Marjańska, A.A. Maudsley, D.J. Meyerhoff, C.E. Mountford, S.J. Nelson, M.N. Pamir, J.W. Pan, A.C. Peet, H. Poptani, S. Posse, P.J.W. Pouwels, E.-M. Ratai, B.D. Ross, T.W.J. Scheenen, C. Schuster, I.C.P. Smith, B.J. Soher, I. Tkáč, D.B. Vigneron, R.A. Kauppinen, Clinical Proton MR Spectroscopy in Central Nervous System Disorders, Radiology 270 (3) (2014) 658–679.
[14] V. Kalia, D.G. Leung, D.B. Sneag, F. Del Grande, J.A. Carrino, Advanced MRI Techniques for Muscle Imaging, Semin Musculoskelet Radiol 21 (4) (2017) 459–469.
[15] M.T. McMahon, A.A. Gilad, J.W.M. Bulte, P.C.M. van Zijl, Chemical Exchange Saturation Transfer Imaging: Advances and Applications, Pan Stanford Publishing, Singapore, 2017, p. 479.
[16] G. Liu, X. Song, K.W. Chan, M.T. McMahon, Nuts and bolts of chemical exchange saturation transfer MRI, NMR Biomed. 26 (7) (2013) 810–828.
[17] A.D. Sherry, M. Woods, Chemical exchange saturation transfer contrast agents for magnetic resonance imaging, Annu. Rev. Biomed. Eng. 10 (2008) 391–411.
[18] E. Vinogradov, A.D. Sherry, R.E. Lenkinski, CEST: From basic principles to applications, challenges and opportunities, J. Magn. Reson. 229 (2013) 155–172.
[19] M. Zaiss, P. Bachert, Chemical exchange saturation transfer (CEST) and MRZ-spectroscopyin vivo: a review of theoretical approaches and methods, Phys. Med. Biol. 58 (22) (2013) R221–R269.
[20] E. Terreno, D.D. Castelli, S. Aime, Encoding the frequency dependence in MRI contrast media: the emerging class of CEST agents, Contrast Media Mol. Imaging 5 (2) (2010) 78–98.
[21] K.M. Jones, A.C. Pollard, M.D. Pagel, Clinical applications of chemical exchange saturation transfer (CEST) MRI, J. Magn. Reson. Imaging 47 (1) (2018) 11–27.
[22] K.M. Ward, A.H. Aletras, R.S. Balaban, A New Class of Contrast Agents for MRI Based on Proton Chemical Exchange Dependent Saturation Transfer (CEST), J. Magn. Reson. 143 (1) (2000) 79–87.
[23] V. Guivel-Scharen, T. Sinnwell, S.D. Wolff, R.S. Balaban, Detection of Proton Chemical Exchange between Metabolites and Water in Biological Tissues, J. Magn. Reson. 133 (1) (1998) 36–45.
[24] S.H. Shin, M.F. Wendland, B. Zhang, A. Tran, A. Tang, M.H. Vandsburger, Noninvasive imaging of renal urea handling by CEST-MRI, Magn. Reson. Med. (2019;0(0).).
[25] K.W.Y. Chan, M.T. McMahon, Y. Kato, G. Liu, J.W.M. Bulte, Z.M. Bhujwalla, D. Artemov, P.C.M. van Zijl, Natural D-glucose as a biodegradable MRI contrast agent for detecting cancer, Magn. Reson. Med. 68 (6) (2012) 1764–1773.
[26] S. Walker-Samuel, R. Ramasawmy, F. Torrealdea, M. Rega, V. Rajkumar, S.P. Johnson, S. Richardson, M. Gonçalves, H.G. Parkes, E. Årstad, D.L. Thomas, R.B. Pedley, M.F. Lythgoe, X. Golay, In vivo imaging of glucose uptake and metabolism in tumors, Nat. Med. 19 (2013) 1067.

[27] T. Jin, S.-G. Kim, Advantages of chemical exchange-sensitive spin-lock (CESL) over chemical exchange saturation transfer (CEST) for hydroxyl– and amine–water proton exchange studies, NMR Biomed. 27 (11) (2014) 1313–1324.
[28] F. Kogan, A. Singh, C. Debrosse, M. Haris, K. Cai, R.P. Nanga, M. Elliott, H. Hariharan, R. Reddy, Imaging of glutamate in the spinal cord using GluCEST, Neuroimage 77 (2013) 262–267.
[29] F. Kogan, M. Haris, A. Singh, K. Cai, C. Debrosse, R.P. Nanga, H. Hariharan, R. Reddy, Method for high-resolution imaging of creatine in vivo using chemical exchange saturation transfer, Magn. Reson. Med. (2013).
[30] A. Pumphrey, Z. Yang, S. Ye, D.K. Powell, S. Thalman, D.S. Watt, A. Abdel-Latif, J. Unrine, K. Thompson, B. Fornwalt, G. Ferrauto, M. Vandsburger, Advanced cardiac chemical exchange saturation transfer (cardioCEST) MRI for in vivo cell tracking and metabolic imaging, NMR Biomed. 29 (1) (2016) 74–83.
[31] L. Chen, P.B. Barker, R.G. Weiss, P.C.M. van Zijl, J. Xu, Creatine and phosphocreatine mapping of mouse skeletal muscle by a polynomial and Lorentzian line-shape fitting CEST method, Magn. Reson. Med. 81 (1) (2019) 69–78.
[32] W. Ling, R.R. Regatte, G. Navon, A. Jerschow, Assessment of glycosaminoglycan concentration in vivo by chemical exchange-dependent saturation transfer (gagCEST), Proc. Natl. Acad. Sci. 105 (7) (2008) 2266.
[33] A. Singh, M. Haris, K. Cai, V.B. Kassey, F. Kogan, D. Reddy, H. Hariharan, R. Reddy, Chemical exchange saturation transfer magnetic resonance imaging of human knee cartilage at 3 T and 7 T, Magn. Reson. Med. 68 (2) (2012) 588–594.
[34] K.W. Chan, T. Yu, Y. Qiao, Q. Liu, M. Yang, H. Patel, G. Liu, K.W. Kinzler, B. Vogelstein, J.W. Bulte, P.C. van Zijl, J. Hanes, S. Zhou, M.T. McMahon, A diaCEST MRI approach for monitoring liposomal accumulation in tumors, Journal of controlled release : official journal of the Controlled Release Society 180 (2014) 51–59.
[35] T. Yu, K.W. Chan, A. Anonuevo, X. Song, B.S. Schuster, S. Chattopadhyay, Q. Xu, N. Oskolkov, H. Patel, L.M. Ensign, P.C. van Zjil, M.T. McMahon, J. Hanes, Liposome-based mucus-penetrating particles (MPP) for mucosal theranostics: demonstration of diamagnetic chemical exchange saturation transfer (diaCEST) magnetic resonance imaging (MRI), Nanomed. Nanotechnol. Biol. Med. 11 (2) (2015) 401–405.
[36] D.L. Longo, W. Dastrù, G. Digilio, J. Keupp, S. Langereis, S. Lanzardo, S. Prestigio, O. Steinbach, E. Terreno, F. Uggeri, Iopamidol as a responsive MRI-chemical exchange saturation transfer contrast agent for pH mapping of kidneys: In vivo studies in mice at 7 T, Magn. Reson. Med. 65 (1) (2011) 202–211.
[37] L.Q. Chen, C.M. Howison, J.J. Jeffery, I.F. Robey, P.H. Kuo, M.D. Pagel, Evaluations of extracellular pH within in vivo tumors using acidoCEST MRI, Magn. Reson. Med. 72 (5) (2014) 1408–1417.
[38] P.Z. Sun, D.L. Longo, W. Hu, G. Xiao, R.H. Wu, Quantification of iopamidol multi-site chemical exchange properties for ratiometric chemical exchange saturation transfer (CEST) imaging of pH, Phys. Med. Biol. 59 (16) (2014) 4493–4504.
[39] R.H. Wu, D.L. Longo, S. Aime, P.Z. Sun, Quantitative description of radiofrequency (RF) power-based ratiometric chemical exchange saturation transfer (CEST) pH imaging, NMR Biomed. 28 (5) (2015) 555–565.
[40] A. Bar-Shir, G.S. Liu, Y.J. Liang, N.N. Yadav, M.T. McMahon, P. Walczak, S. Nimmagadda, M.G. Pomper, K.A. Tallman, M.M. Greenberg, P.C.M. van Zijl, J.W. M. Bulte, A.A. Gilad, Transforming Thymidine into a Magnetic Resonance Imaging Probe for Monitoring Gene Expression, J. Am. Chem. Soc. 135 (4) (2013) 1617–1624.
[41] X. Yang, X. Song, Y. Li, G. Liu, S. Ray Banerjee, M.G. Pomper, M.T. McMahon, Salicylic Acid and Analogues as diaCEST MRI Contrast Agents with Highly Shifted Exchangeable Proton Frequencies, Angew. Chem. Int. Ed. 52 (31) (2013) 8116–8119.
[42] X. Song, X. Yang, S. Ray Banerjee, M.G. Pomper, M.T. McMahon, Anthranilic acid analogs as diamagnetic CEST MRI contrast agents that feature an intramolecular-bond shifted hydrogen, Contrast Media Mol. Imaging 10 (1) (2015) 74–80.
[43] X. Yang, X. Song, S. Ray Banerjee, Y. Li, Y. Byun, G. Liu, Z.M. Bhujwalla, M.G. Pomper, M.T. McMahon, Developing imidazoles as CEST MRI pH sensors, Contrast Media Mol. Imaging 11 (4) (2016) 304–312.
[44] X. Zhang, Y. Yuan, S. Li, Q. Zeng, Q. Guo, N. Liu, M. Yang, Y. Yang, M. Liu, M.T. McMahon, X. Zhou, Free-base porphyrins as CEST MRI contrast agents with highly upfield shifted labile protons, Magn. Reson. Med. 82 (2) (2019) 577–585.
[45] A. Bar-Shir, G. Liu, K.W.Y. Chan, N. Oskolkov, X. Song, N.N. Yadav, P. Walczak, M.T. McMahon, P.C.M. van Zijl, J.W.M. Bulte, A.A. Gilad, Human Protamine-1 as an MRI Reporter Gene Based on Chemical Exchange, ACS Chem. Biol. 9 (1) (2014) 134–138.
[46] A.A. Gilad, M.T. McMahon, P. Walczak, P.T. Winnard, V. Raman, H.W.M. van Laarhoven, C.M. Skoglund, J.W.M. Bulte, P.C.M. van Zijl, Artificial reporter gene providing MRI contrast based on proton exchange, Nat. Biotechnol. 25 (2) (2007) 217–219.
[47] M.T. McMahon, A.A. Gilad, M.A. DeLiso, S.M. Cromer Berman, J.W.M. Bulte, P.C. M. van Zijl, New "multicolor" polypeptide diamagnetic chemical exchange saturation transfer (DIACEST) contrast agents for MRI, Magn. Reson. Med. 60 (4) (2008) 803–812.
[48] C.T. Farrar, J.S. Buhrman, G. Liu, A. Kleijn, M.L.M. Lamfers, M.T. McMahon, A.A. Gilad, G. Fulci, Establishing the Lysine-rich Protein CEST Reporter Gene as a CEST MR Imaging Detector for Oncolytic Virotherapy, Radiology 275 (3) (2015) 746–754.
[49] R. Fu, W.W. Brey, K. Shetty, P. Gor'kov, S. Saha, J.R. Long, S.C. Grant, E.Y. Chekmenev, J. Hu, Z. Gan, M. Sharma, F. Zhang, T.M. Logan, R. Brüschweller, A. Edison, A. Blue, I.R. Dixon, W.D. Markiewicz, T.A. Cross, Ultra-wide bore 900MHz high-resolution NMR at the national high magnetic field laboratory, J. Magn. Reson. 177 (1) (2005) 1–8.
[50] G. Liu, A.A. Gilad, J.W. Bulte, P.C. van Zijl, M.T. McMahon, High-throughput screening of chemical exchange saturation transfer MR contrast agents, Contrast Media Mol. Imaging 5 (3) (2010) 162–170.
[51] M. Kim, J. Gillen, B. Landman, J. Zhou, P. van Zijl, Water saturation shift referencing (WASSR) for chemical exchange saturation transfer (CEST) experiments, Magn. Reson. Med. 61 (6) (2009) 1441–1450.
[52] K. Pavuluri, I. Manoli, A. Pass, Y. Li, H.J. Vernon, C.P. Venditti, M.T. McMahon, Noninvasive monitoring of chronic kidney disease using pH and perfusion imaging, Sci. Adv. 5 (8) (2019) eaaw8357.
[53] M.T. McMahon, A.A. Gilad, J. Zhou, P.Z. Sun, J.W. Bulte, P.C. van Zijl, Quantifying exchange rates in chemical exchange saturation transfer agents using the saturation time and saturation power dependencies of the magnetization transfer effect on the magnetic resonance imaging signal (QUEST and QUESP): Ph calibration for poly-L-lysine and a starburst dendrimer, Magn. Reson. Med. 55 (4) (2006) 836–847.
[54] N. Goffeney, J.W. Bulte, J. Duyn, L.H. Bryant Jr., P.C. van Zijl, Sensitive NMR detection of cationic-polymer-based gene delivery systems using saturation transfer via proton exchange, J. Am. Chem. Soc. 123 (35) (2001) 8628–8629.
[55] T. Jin, P. Wang, X. Zong, S.-G. Kim, MR imaging of the amide-proton transfer effect and the pH-insensitive nuclear overhauser effect at 9.4 T, Magn. Reson. Med. 69 (3) (2013) 760–770.
[56] D. Street, J. Bangsbo, C. Juel, Interstitial pH in human skeletal muscle during and after dynamic graded exercise, The Journal of physiology 537 (Pt 3) (2001) 993–998.
[57] J. Stabinska, P. Neudecker, A. Ljimani, H.J. Wittsack, R.S. Lanzman, A. Muller-Lutz, Proton exchange in aqueous urea solutions measured by water-exchange (WEX) NMR spectroscopy and chemical exchange saturation transfer (CEST) imaging in vitro, Magn. Reson. Med. 82 (3) (2019) 935–947.
[58] M. Haris, A. Singh, K. Cai, F. Kogan, J. McGarvey, C. Debrosse, G.A. Zsido, W.R. Witschey, K. Koomalsingh, J.J. Pilla, J.A. Chirinos, V.A. Ferrari, J.H. Gorman, H. Hariharan, R.C. Gorman, R. Reddy, A technique for in vivo mapping of myocardial creatine kinase metabolism, Nat. Med. 20 (2) (2014) 209–214.
[59] C. DeBrosse, R.P.R. Nanga, N. Wilson, K. D'Aquilla, M. Elliott, H. Hariharan, F. Yan, K. Wade, S. Nguyen, D. Worsley, C. Parris-Skeete, E. McCormick, R. Xiao, Z. Z. Cunningham, L. Fishbein, K.L. Nathanson, D.R. Lynch, V.A. Stallings, M. Yudkoff, M.J. Falk, R. Reddy, S.E. McCormack, Muscle oxidative phosphorylation quantitation using creatine chemical exchange saturation transfer (CrCEST) MRI in mitochondrial disorders, JCI insight 1 (18) (2016) e88207.
[60] P.Z. Sun, Y. Wang, G. Xiao, R.H. Wu, Simultaneous experimental determination of labile proton fraction ratio and exchange rate with irradiation radio frequency power-dependent quantitative CEST MRI analysis, Contrast Media Mol. Imaging 8 (3) (2013) 246–251.
[61] J.J. Chung, T. Jin, J.H. Lee, S.G. Kim, Chemical exchange saturation transfer imaging of phosphocreatine in the muscle, Magn. Reson. Med. 81 (6) (2019) 3476–3487.
[62] R.M. Filler, J.B. Das, G.M. Haase, P.K. Donahoe, Muscle surface pH as a monitor of tissue perfusion and acid-base status, J. Pediatr. Surg. 6 (5) (1971) 535–542.
[63] O.S. Ipsiroglu, C. Stromberger, J. Ilas, H. Hoger, A. Muhl, S. Stockler-Ipsiroglu, Changes of tissue creatine concentrations upon oral supplementation of creatine-monohydrate in various animal species, Life Sci. 69 (15) (2001) 1805–1815.